DEGREE PROJECT FOR MASTER OF SCIENCE WITH SPECIALIZATION IN MANUFACTURING
DEPARTMENT OF ENGINEERING SCIENCE
UNIVERSITY WEST

Laser Metal Powder Deposition of Austenitic Stainless Steel on Spheroidal Graphite Cast Iron

- A corrosion resistant coating for the Food & Beverage Industry -

Alejandro Molina Griggs

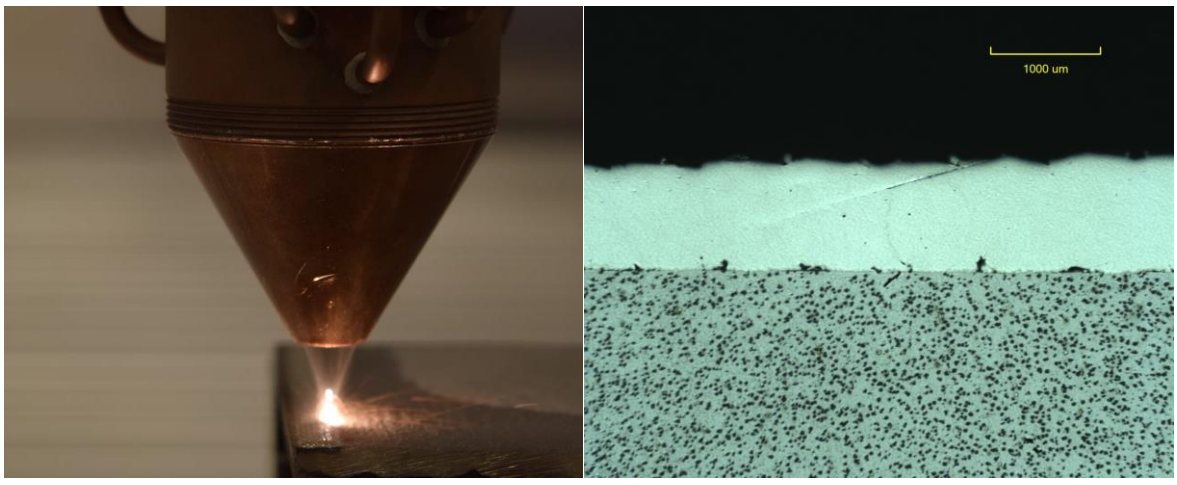

UNIVERSITY WEST

Summary

Spheroidal graphite cast iron is a material widely used in the industry for the manufacturing of all kind of covers and protective casings thanks to its good combination of mechanical properties, processability and cost. When cast iron components are put into service in corrosive environments the most common approach to protect the components is painting them.

The protective painting has been found to flake off with time when aggressive washing procedures, such as the ones used in the Food & Beverage industry, are applied several times. In this project, the coating of cast iron with a corrosion resistant AISI 316L stainless steel by Laser Metal Powder Deposition has been studied as an alternative protection against corrosion.

Several samples with different combinations of substrate preparation, number of layers and surface conditions were produced and analysed by optical microscopy, scanning electron microscopy, energy dispersive X-ray spectroscopy, wash down tests and salt spray chamber corrosion tests.

Main results show that the diffusion of carbon from the carbon-rich cast iron to the stainless steel coating, which would have a negative effect on the corrosion resistant properties, was significantly low as a result of the low penetration and dilution achieved during the laser metal powder deposition process. The deposited stainless steel coatings successfully protected the substrate during the corrosion tests and the integrity of the coatings is not expected to fail during the washing producers applied in the industry.

Date:	August 21, 2018
Author:	Alejandro Molina Griggs
Examiner:	Ph.D. Joel Andersson
Supervisor:	Ph.D. María Asunción Valiente Bermejo
Advisor:	Ph.D. Jian Quin, ABB Corporate Research
Program:	Master in Manufacturing Engineering, 60 HE credits
Main field of study:	Mechanical Engineering
Title in Swedish	**Laser metalldeponering av AISI 316L på Segjärn – En korrosionsbeständig beläggning för livsmedelsindustrin –**
Credits:	15 Higher Education credits (see the course syllabus)
Keywords	LMPD, AISI 316L, Cast Iron, Corrosion Resistant Coating, F&B Industry
Publisher:	University West, Department of Engineering Science, S-461 86 Trollhättan, SWEDEN Phone: + 46 520 22 30 00 Fax: + 46 520 22 32 99 Web: www.hv.se

Preface

There are many persons and institutions which I would like to thank for making this project possible.

First, I would like to thank ABB Corporate Research for choosing me for such an interesting project and for providing all the necessary financial resources to successfully complete it. All my colleagues at ABB helped me to quickly feel integrated and part of the group, but I want to particularly express my gratitude to Jian for always finding the time to help me out and answer all my questions.

I want to thank Högskolan Väst and its Production Technology Centre for a wonderful year and for giving me completely free access to all the equipment and materials which I needed to finish this project. I consider myself very lucky to have been helped by Kjell Hurtig, whose vast experience and knowledge of the involved equipment and processes proved critical for the project success.

I am very glad to state that this master thesis work would have not been possible without the active collaboration of Dr. Valiente, who trusted me to develop this interesting research topic. Thank you for your sincere involvement since the beginning of the project, for all your help and for your patience with my too often stubborn personality.

I am deeply grateful to my company, B. Braun, for allowing me to fulfil my dream of studying and living in another European culture without being afraid of losing my position or hindering my future career.

Last but not least, I want to dedicate this thesis work to my grandfather José Molina who passed away while I was in Sweden and who always encouraged me to keep on studying. I wish that you were here to see that I made it and I came back home.

Affirmation

This master degree report, ***Laser Metal Powder Deposition of AISI 316L on Spheroidal Graphite Cast Iron***, was written as part of the master degree work needed to obtain a Master of Science with specialization in manufacturing degree at University West. All material in this report, that is not my own, is clearly identified and used in an appropriate and correct way. The main part of the work included in this degree project has not previously been published or used for obtaining another degree.

_____ _____

Signature by the author Date

Alejandro Molina Griggs

Contents

Contents

Symbols and glossary

AM	Additive Manufacturing
ASTM	American Society for Testing and Materials
EDS	Energy Dispersive X-ray Spectroscopy
FN	Ferrite Number
F&B	Food and beverage
IP	Ingress Protection
LMPD	Laser Metal Powder Deposition
LMWD	Laser Metal Wire Deposition
SEM	Scanning Electron Microscopy
SS	Stainless Steel

1 Introduction

The purpose of this project is to investigate the feasibility of using Laser Metal Powder Deposition to deposit a corrosion resistant coating of austenitic stainless steel on a ductile cast iron substrate.

The main research question is: is it possible to directly deposit stainless steel powder on cast iron without the use of an intermediate nickel-rich buffer layer? The development of a LMPD process which allows to directly deposit stainless steel layers on cast iron has been considered in this project.
Some sub research questions are derived from the main research question:
- Is the initial substrate surface condition a key parameter to achieve the desired quality in the coating?
- How many deposited layers are necessary to guarantee a pure austenitic stainless steel surface with no carbon diffusion from the carbon-rich cast iron substrate?
- Is it beneficial in terms of corrosion resistance to remelt the surface of the last stainless steel layer?

The deposited corrosion resistant coatings and related process parameters developed in this project are intended to protect the outer cover of ABB robots which will be put into service in the food and beverage industry.

The testing plan and acceptance criteria have been established in accordance with ABB specifications. The coatings should be able to withstand a high-pressure steam wash-down test equivalent to an IP69K level (ISO 20653:2013 Road Vehicles – Degrees of protection IP Code – Protection of electrical equipment against foreign objects, water and access) [1] and pass a laboratory accelerated cyclic corrosion test (Volvo Standard VCS 1027,1449) [2]. The aim of this project is to develop a coating with a sound austenitic microstructure and a low substrate-coating dilution to ensure a high corrosion resistance level and reliable mechanical properties. As a thesis work with a strong connection to industry, the developed coating must fulfill the above-mentioned tests and gives an answer to ABB expectations in the most industry-friendly possible way.

2 Background

2.1 Motivation

The automation and robotization of manufacturing lines is a current trend in most industrial fields, especially in developed countries. The F&B industry, which usually involves high volumes of units that must be quickly processed and distributed, is not an exception to this tendency [3].

Due to the high potential public health risks related to the food and beverage industry, regulations and design guidelines have been implemented in the last decades in an attempt to minimize these risks [4]. In order to fulfil the regulations and maintain a general cleanliness level, the usage of washing and cleaning procedures involving high temperatures, pressure and chemical products are common and widespread in the manufacturing plants.

Especial attention is paid to all pieces of equipment that may come into direct contact with a product before its final packaging, including manipulating robots, which are cleaned with a higher frequency and usually with more aggressive procedures than other elements in the factory. The frequent cleaning of the manipulating robots, along with the corrosive behavior of organic matter, create a corrosive environment that must be taken into account prior to the selection and installation of the robotic system.

The outer casings of industrial robots are typically painted to improve their visual appearance and their corrosion resistance, but the painted layer has been found to flake off during some of the cleaning processes used in the F&B industry. This introduces the necessity to find a new industrial friendly way to protect the robots from corrosion with both a material and manufacturing process which produce a surface that fulfills the requirements to be in contact with food.

2.2 Materials and processes

As the main function of the outer cover of a robotic arm is to seal the rest of the system from the environment and it is not designed to be subjected to high mechanical stresses, cast iron is the material of choice of most robot manufacturers for this purpose. Cast iron is a well-known and cheap material which can be easily casted into its final shape requiring very little (or none) post-processing. As an example, the cast iron covers involved in this project are painted and put into service in the as-cast condition.

Making the protective cover of the robot of a corrosion resistant material such as stainless steel or aluminum would be indeed a solution, but due to the afore mentioned reasons the usage of cast iron instead of more expensive materials is preferable as long as another solution to the corrosion issue is found.

Despite their many advantages and being the material of choice for all kinds of outer casings and protective covers for industrial applications, cast irons present several difficulties during welding and cladding processes. Their characteristic high carbon percentage and complex microstructure makes them particularly susceptible to manufacturing processes involving heat. *Figure 1* [5] shows the effects of welding ductile cast iron with a nickel rich alloy with or without a preheat treatment and illustrates how the final microstructure of cast irons is closely related to its thermal history. In the case of the sample that was preheated (b), the cooling rate after welding was slower so the carbon contained in the graphite nodules had time to diffuse to areas with a lower carbon content. As a result, the desirable spheroidal geometry of the graphite nodules was lost in a much wider area of the HAZ.

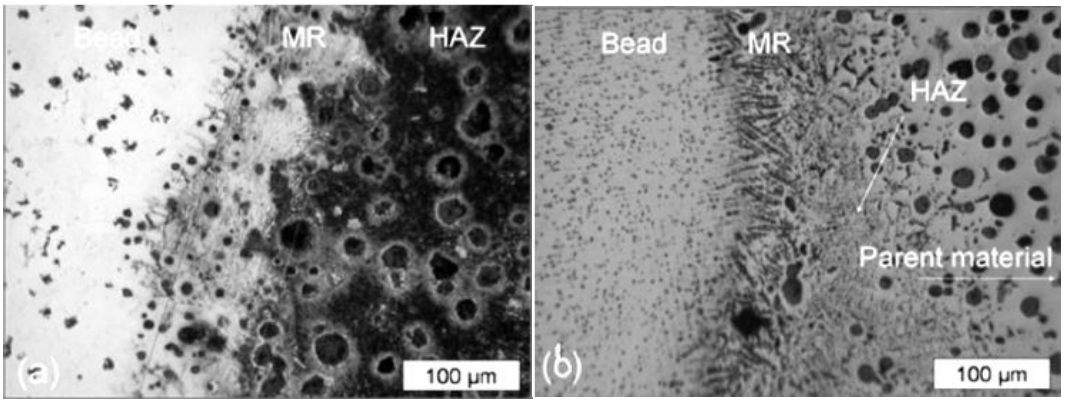

Figure 1, Optical Images of ductile cast iron welded with a 57.2% Ni-Fe electrode [5]:

(a) as-welded without preheat treatment *(b) as-welded with preheat treatment*

The reason why cast irons are so susceptible to welding processes is because, upon rapid cooling, undesirable brittle phases such as martensite and iron carbides will form, and the microstructure of the HAZ will be modified [6].
The microstructure of spheroidal graphite cast iron, the chosen substrate material for this project, is even more sensible to the effects of heat than other types of cast iron. Apart of the formation of brittle phases and related microstructural changes, the spheroidal geometry of the graphite has been found to be completely changed. The loss of the spheroidal geometry in the HAZ, and the loss of the improved mechanical properties related to it, cannot be avoided and can only be restored with a high temperature postweld heat treatment. The most effective way to retain the desirable mechanical properties of spheroidal graphite cast iron is decreasing the heat input and therefore the width of the HAZ as much as possible [9] [10] [11]. If the heat input cannot be further minimized due to process limitations, it is possible to reduce the cooling rate with a preheat treatment before welding.

The chosen corrosion resistance material that will be deposited on the cast iron is, for several reasons, an AISI 316L austenitic stainless steel grade.
Austenitic stainless steels are used world-wide for corrosion resistance applications in all kind of environments and industrial sectors. Among the different austenitic stainless steel grades, the AISI 316L grade is probably the most used and well-known grade for pipelines, deposits and welded structures in the chemical, pharmaceutical and F&B industries [14] [15].

Austenitic stainless steels are easier to weld than cast irons and other steel families, and the AISI 316L was specially developed for welding purposes. The "L" of the AISI 316L nomenclature means that the carbon content is lower (< 0.03 wt%) than the standard AISI 316, so all welding difficulties related to carbon content, including sensitization, are reduced. It is possible to produce specimens and claddings of austenitic stainless steels with additive manufacturing techniques which have the same or better corrosion resistance than conventionally produced components. For example, J. Dutta Majumdar et al. demonstrated that a multiple-layer laser cladding of 316L had a superior resistance against pitting corrosion than a conventionally produced 316L component [16]. Qi Chiao et al. concluded that a 316L component manufactured through selective laser melting also had a superior corrosion resistance than a wrought component [17].

The coating method selected for this project, LMPD, is commonly used for the deposition of claddings and it is characterized for generating a low heat input in comparison to other direct metal deposition systems.
If a coaxial powder feeding nozzle is used, the laser focal point can be directed to the point where the powder converges above the substrate (*Figure 2*). Doing so, the amount of laser energy received by the substrate is attenuated and the molten powder can be spread over a wider area of the substrate. The heat input and the dilution of the powder with the substrate are significantly reduced in comparison to other methods, such as arc welding or LMWD [12]. Its low heat input positions LMPD as one of the best alternatives for the cladding of heat sensitive materials such as spheroidal graphite cast iron.

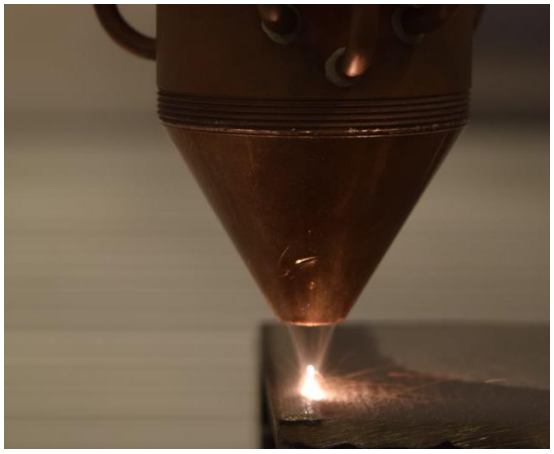

Figure 2, Coaxial LMPD feeding nozzle used in the project

When cladding a material which can develop a microstructure with hard and brittle phases such as spheroidal cast iron , the deposition of two or more layers of metal powder is expected to have a beneficial influence on the microstructure and mechanical properties of the substrate HAZ produced by the first layer. Due to the high cooling rate caused by the heat sink effect of the cold thick cast iron plate, a high percentage of untempered martensite can be anticipated. The heat input of successive layers will temper some of the martensite and reduce residual stresses [8] [9] [13].

When a corrosion resistance coating involving dissimilar materials such as cast iron and stainless steel is deposited, minimizing the dilution and diffusion between the cladding material and the substrate is desirable. A low substrate temperature will result in a lower

penetration of the molten powder and a faster solidification, therefore reducing the dilution and diffusion time between the two materials [7] [8]. Consequently, it is not a common practice to preheat the substrate prior to the deposition of a corrosion resistance coating. Additionally, preheating a component that is going to be cladded by LMPD can be difficult because introducing and clamping the component in the LMPD machine can be cumbersome.

During the additive manufacturing process of austenitic stainless steel components, a sensitization risk can be introduced if the component is maintained at elevated temperatures or let to cool down at a rate where it will stay in the sensitization temperature range (500-800 ºC) for a sufficient time. Even with its very low carbon content, an additive manufactured AISI 316L specimen can become sensitized and intergranular corrosion will appear with time [20][21]. Because of the high cooling rates related to the LMPD method, the sensitization risk is greatly reduced and the corrosion resistance of the samples produced in this project is not expected to be affected by it.

The surface roughness of AM samples can be drastically improved by laser polishing [23][24][25]. To further increase the corrosion resistance and visual appearance of additive manufactured (AM) components, laser polishing or laser remelting of the last deposited layer can be performed to improve the surface roughness. A lower surface roughness improves the resistance against pitting corrosion in most metals, including stainless steels [22].

In general terms, the weldability of cast irons and austenitic stainless steel is considered to be poor. A nickel-rich buffer layer is commonly applied on the cast iron prior to the stainless steel to reduce the appearance of welding related problems and to guarantee a reliable bonding. Nickel increases the ductility of the weld, does not form brittle compounds with carbon and reduces the diffusion of carbon towards the iron, making martensite formation and carbides formation less likely [6][26][5].

Nickel-rich alloys are expensive and it is the purpose of this work to evaluate if, for certain applications such as the cladding of the outer cover of ABB robots where no significant mechanical stresses are expected, the weld quality of the deposits obtained without the use of a buffer layer could be enough to fulfill its duty during the complete service life of the component. No articles or previous academic work regarding the direct LMPD of AISI 316L SS on cast iron has been found during the literature review.

3 Experimental Methodology

A coating, containing from one to three layers of 316L stainless steel, was deposited on spheroidal graphite cast iron plates. In some cases, a nickel-rich buffer layer was deposited on the cast iron substrate prior to the stainless steel to compare the effects of having a buffer layer on the final coating. The substrate surface of most samples was grit blasted, but some of them were machined to produce a completely flat and oxide-free surface. All coatings were deposited using the same LMPD equipment and process parameters.

The cross-section of the produced samples was analysed by Optical Microscopy (OM), Scanning Electron Microscopy (SEM) and Energy Dispersive X-Ray Spectroscopy (EDS). The samples were subjected to two wash-down tests involving high-pressure steam and a corrosion resistance test. The ferrite content of the coating surface was measured with a Feritoscope.

3.1 Materials

Substrate

Material: EN GJS-500-7, spheroidal graphite cast iron plates 80 x 80 x 8 mm (length, width, thickness). Chemical composition (wt %) provided by the supplier:

Fe	C	Si	Mn	S	P	Mg
Bal.	3.25-3.75	2.40-3.00	0.10-0.30	0.005-0.020	0.015-0.08	0.04-0.07

Buffer layer

Material: Inconel 718, nickel-chromium superalloy in powder form.
Powder Size: 45-75 μm. Chemical composition (wt %) provided by the supplier:

Ni	Cr	Fe	Nb	Mo	Ti	Al	Si	Mn	C	Co	Cu	P	B	S
53.9	18.7	18	5.16	2.99	0.94	0.41	0.08	0.07	0.040	<0.01	<0.01	<0.003	<0.001	0.001

Coating

Material: AISI 316L, austenitic stainless steel in powder form. Powder size: 45-75 μm. Chemical composition (wt %) provided by the supplier:

Fe	Cr	Ni	Mo	C	Si	Mn	S	P	N
67.77	16.9	12.38	2.53	0.014	0.69	1.45	0.007	0.02	0.053

3.2 Manufacturing equipment and process parameters

For the samples with a machined surface condition, 1.5 mm of material were removed with a *SAJO VF 52 STR* milling machine, using a *SECO Octomill Skäarstorlek-05* cutting tool with a spindle speed of 500 rpm and a feed of 1.6 mm/rev.

Robotized Laser metal powder deposition

Robotic system: *INSEL Overhead Gantry M40 CNC-Milling Machine* modified with a co-axial annular powder nozzle and a laser optic (*Fig.3*). The laser source was a *IPG Photonics* Ytterbium 6 kW fiber laser and the powder nozzle was connected to a *Uniquecoa*t volumetric powder feeder. The powders were sieved before being loaded to the powder feeder to ensure that there were no particles over 75 μm.
Auxiliary equipment: nozzle water cooling system, argon gas supply system.

Process parameters:

The process parameters are summarized in Table 1 and described below:

Nozzle-substrate distance: distance between the final part of the nozzle where the powder particles are ejected and the substrate.

Height increment per layer: increase of the height of the nozzle (Z axis) each time a new layer is going to be deposited. Intended to maintain nozzle-substrate distance dependent parameters constant.

Overlap: increase in the width direction (X axis) of the sample each time the deposition of a bead is finished.
Laser standoff distance: distance between the laser focus point and the substrate. A positive value means that the laser focus point is above the substrate.

Laser spot diameter: diameter of the laser beam at the substrate surface level. It is affected by the laser standoff distance.

Table 1, LMPD Process parameters

	Inconel 718	AISI 316L	Remelting
Powder feeding rate (g/min)	6.2	6	0
Shielding gas flow (L/min)	3	3	3
Carrying gas flow (L/min)	12	12	0
Laser power (W)	1000	1000	650
Travel Speed (mm/s)	17.5	17.5	17.5
Nozzle-substrate Distance (mm)	12.5	12.5	12.5
Height increment per layer (mm)	0.8	1.2	0
Overlap (mm)	0.8	0.8	0.8
Laser Standoff distance (mm)	7.5	7.5	7.5
Laser Spot Diameter (mm)	1.5	1.5	1.5

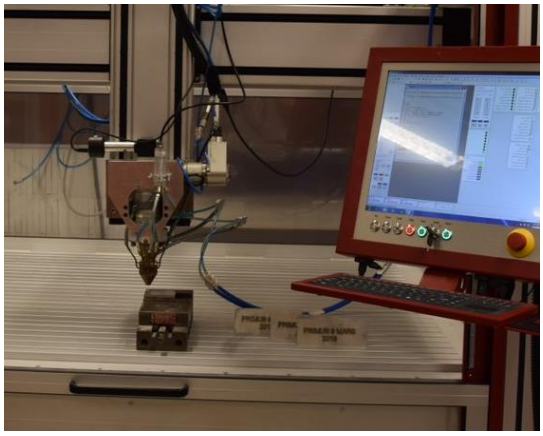

Figure 3, Robotized LMPD system

3.3 Sampling

A total of 16 samples were produced and summarized in Figure 4. They were classified according to the presence of a nickel-rich buffer layer, surface condition, number of stainless steel layers and if the last deposited layer was laser remelted or left as-deposited.

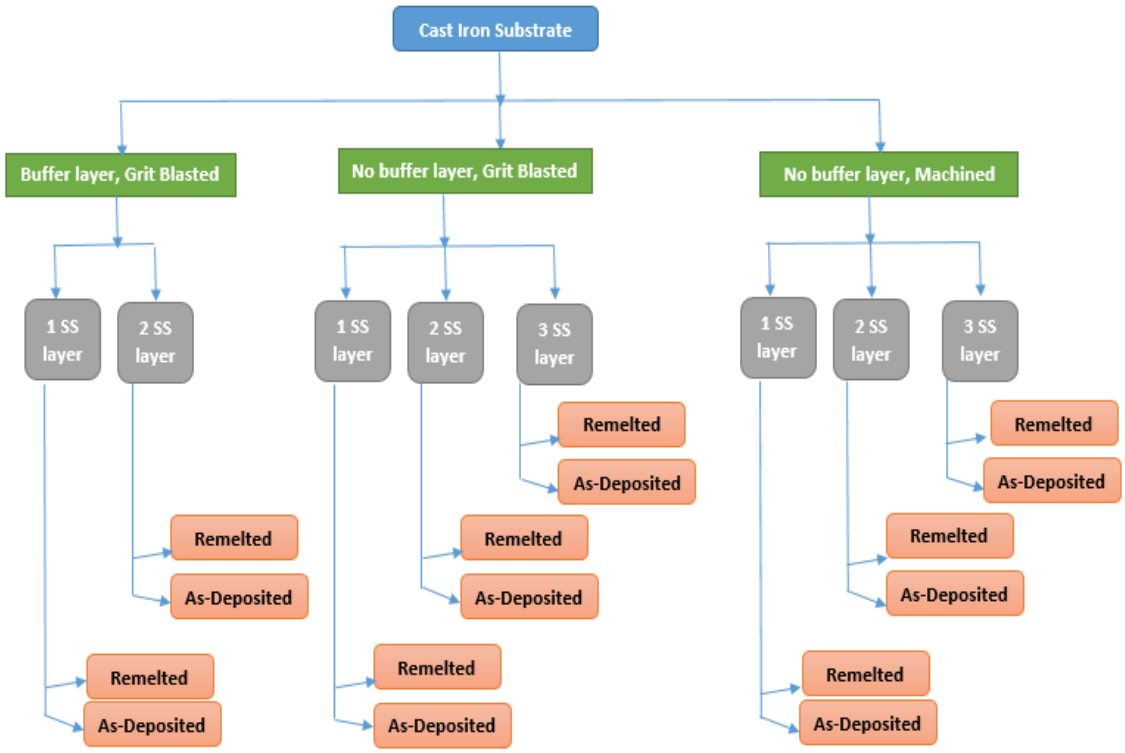

Figure 4, Sampling Plan Summary

3.4 Testing

3.4.1 Microscopy

Prior to microscopy, samples were prepared as follows. They were manually cut with an abrasive cutter. A 1 cm wide strip was cut from each sample, and specimens were then cut out from the central part of the 1 cm wide strips.
The cut specimens were then hot mounted, polished and ground following conventional metallographic preparation procedures. The chosen polishing and grinding process parameters were indicated for the preparation of hard ferrous alloys because cast iron accounted for the majority of the specimen surface.
The mounted and polished specimens were etched with Kalling's II, a chemical agent specially indicated for the metallographic analysis of austenitic stainless steel. The dwelling time of the etching agent was 3 seconds.

Optical Microscopy

Equipment: Olympys BX60M
Software: Lumenera Infinity Analyze software package.

Lower magnifications (x12.5, x50) were used to perform macroscopic inspections and measurements. Images of the several interphases, defects and microstructures were taken of all specimens with the three highest magnifications (x200, x500, x1000).
The average cell size of the resulting microstructure was calculated following the General Interception Procedure for average grain size established by ASTM E112-12 and using equation A1.4 of the annexes [27].

Scanning Electron Microscope, Energy Dispersive X-Ray Spectroscopy

A SEM (Hitachi TM300 Tabletop Microscope) with integrated EDS was used to obtain qualitative data about the chemical composition of the different layers, interphases and surface particles.

3.4.2 Wash down test

The samples were washed down twice, after and before the corrosion test, with a jet of pressurized water (Kärcher Super Class Hot water cleaner) following the necessary steps and parameters to obtain an IP69K protection level.
The purpose of this test is to assess the adherence of the coating to the substrate and if the coating shows a tendency to flake off when high pressures are applied to its surface. Three different water pressures (50, 70, 100 bars) combined with four different angles of incidence of the water jet (0º, 30º, 60º, 90º) were applied to each sample per test. The exposure time for each pressure-angle combination was 30 seconds and the nozzle-sample distance was between 10-15 cm. The test parameters for the wash down test are summarized in *Table 2*.

Table 2, Wash Down Test Parameters

	50 bars	70 bars	100 bars
0º	30 s	30 s	30 s
30º	30 s	30 s	30 s
60º	30 s	30 s	30 s
90º	30 s	30 s	30 s

3.4.3. Corrosion test

All samples were subjected to a corrosion resistance test in a temperature-humidity controlled salt spray chamber. To pass the corrosion test, the samples should be free of any pitting corrosion signs after being exposed to the following one-week long corrosion cycle established by Volvo's Standard VCS 1027,1449:
- Five 24 h cycles consisting of a 6 h wet phase at room temperature with intermittent exposure to a salt solution (0.5 % NaCl), a 2.5-h transition phase with drying under climate control and a 15.5 h phase with constant temperature and humidity (50 °C, 70 % RH).
- A 48 h final phase under continued constant climate control (50 °C, 70 % RH).

3.4.4. Ferrite measurement

Equipment: Fischer Feritscope FMP30
The ferrite number (FN) in the coating surface was measured. As austenite is paramagnetic, the FN could be used to estimate the amount of delta ferrite in the stainless steel (SS) coatings. It is possible that the magnetic field generated by the ferrite and/or martensite content of the cast iron substrate had an influence on the FN obtained values, particularly for samples with only one deposited layer.

4. Results and Discussion

4.1. Microscopy

4.1.1. Optical microscopy

The images obtained with the optical microscope were the most important data to determine the nature and quality of the interphases, the type of defects in the coating and the resulting microstructure.

Substrate-Coating interphase:
The penetration depth of the weld was found to be very low. The low penetration of the deposited layer is expected to be caused by the laser energy attenuation factor related to having the laser focus point and the powder convergence point some distance above the substrate. In *Figures 4 and 5* the shallow penetration of the first layer can be appreciated in comparison to the total thickness of the deposited coating. The border between the cast iron and the first SS layer is clearly defined, suggesting that the two materials only mixed in a significantly thin interphase.

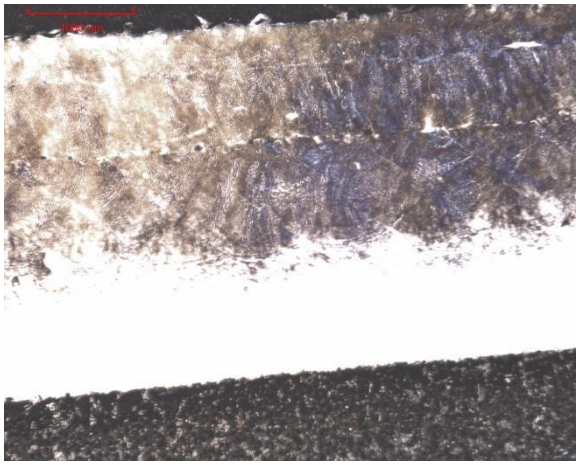

Figure 4, general picture of a machined surface with 3 layers of SS sample.

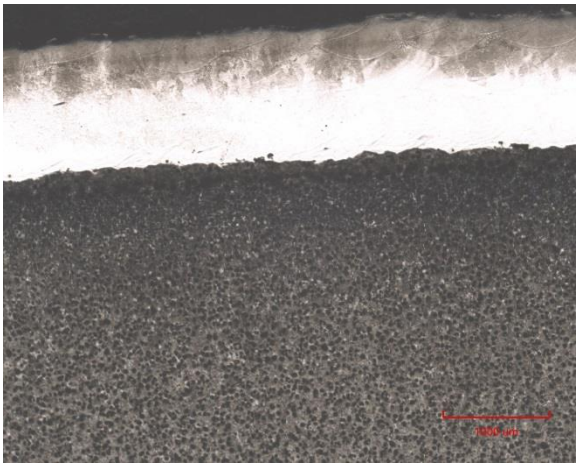

Figure 5, general picture of a sand blasted surface with 1 layer of SS sample.

The resulting substrate-coating interphase was so thin and unclear that it was difficult to precisely measure its thickness in many samples. For the samples where it was possible to obtain a reasonable precise measurement, the thickness of the interphase was estimated to be between 20-50 μm. *Figures 6* is an example of the interphase thickness measurement.

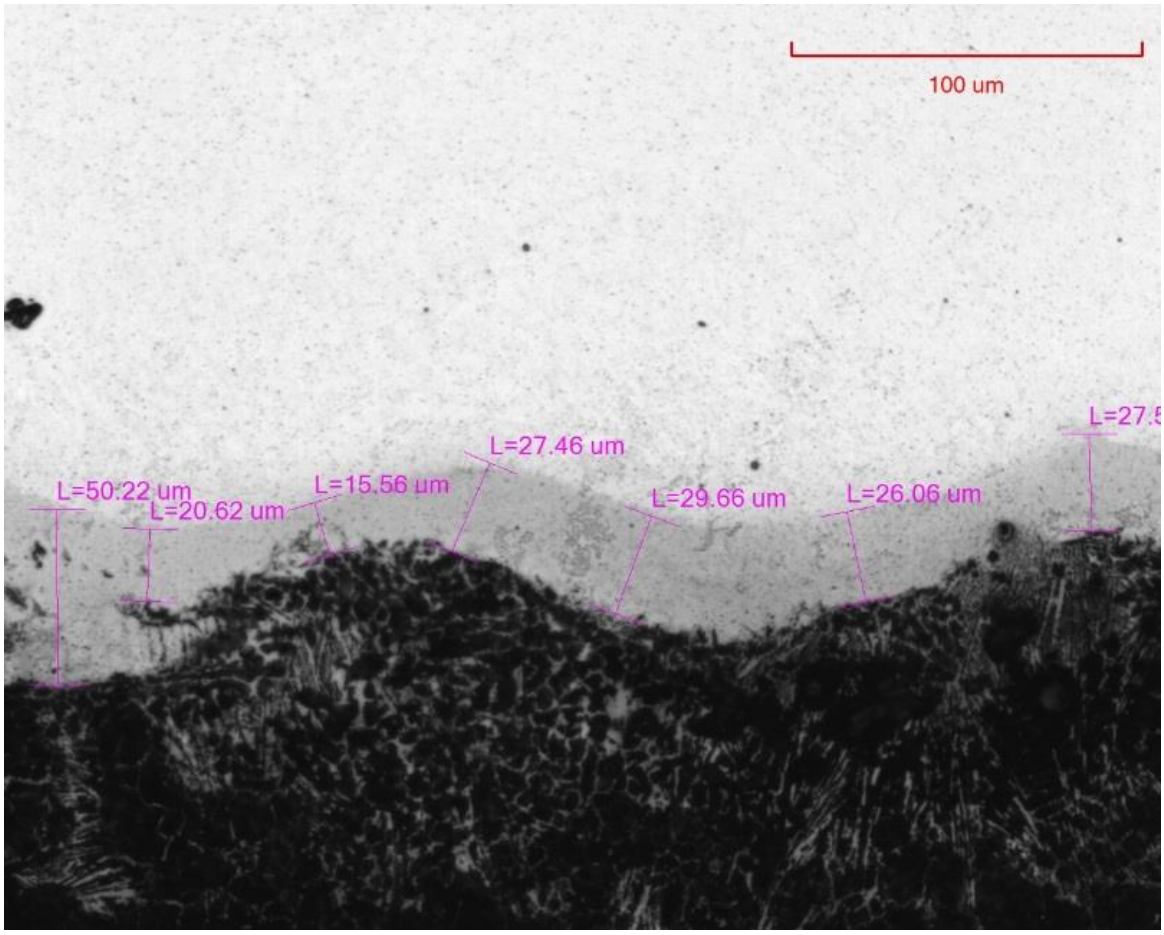

Figure 6, substrate-coating interphase of a grit blasted sample with 2 SS layers

Thickness of the deposited layers:

The thickness of the deposited layers is similar in all samples, regardless of the number of deposited layers or if the last layer was remelted. The thickness of the buffer layer has been determined to be between 800-900 μm, and of 1050-1200 μm for the SS layers.

Figures 7and 8 show two equal samples except for the remelted surface condition. The laser remelting process does not seem to influence on the thickness of the layers.

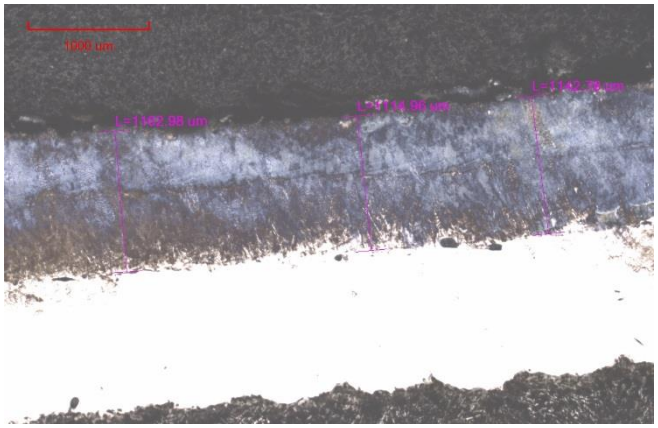

Figure 7, layer thickness of a machined sample with 2 SS layers

Measured thickness: 1162 μm, 1114 μm and 1142 μm

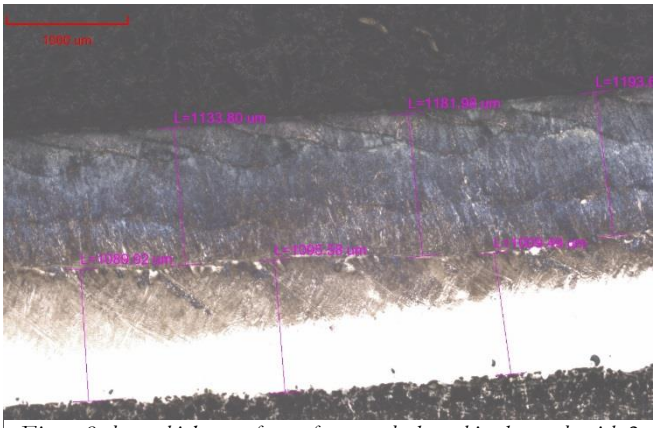

Figure 8, layer thickness of a surface remelted machined sample with 2 SS layers

Measured thickness: 1133 μm, 1181 μm and 1193 μm

Figures 9 and 10 display several measurements of the thickness of SS layers. The thickness of the layer is not affected by the deposition order (first, second or third).

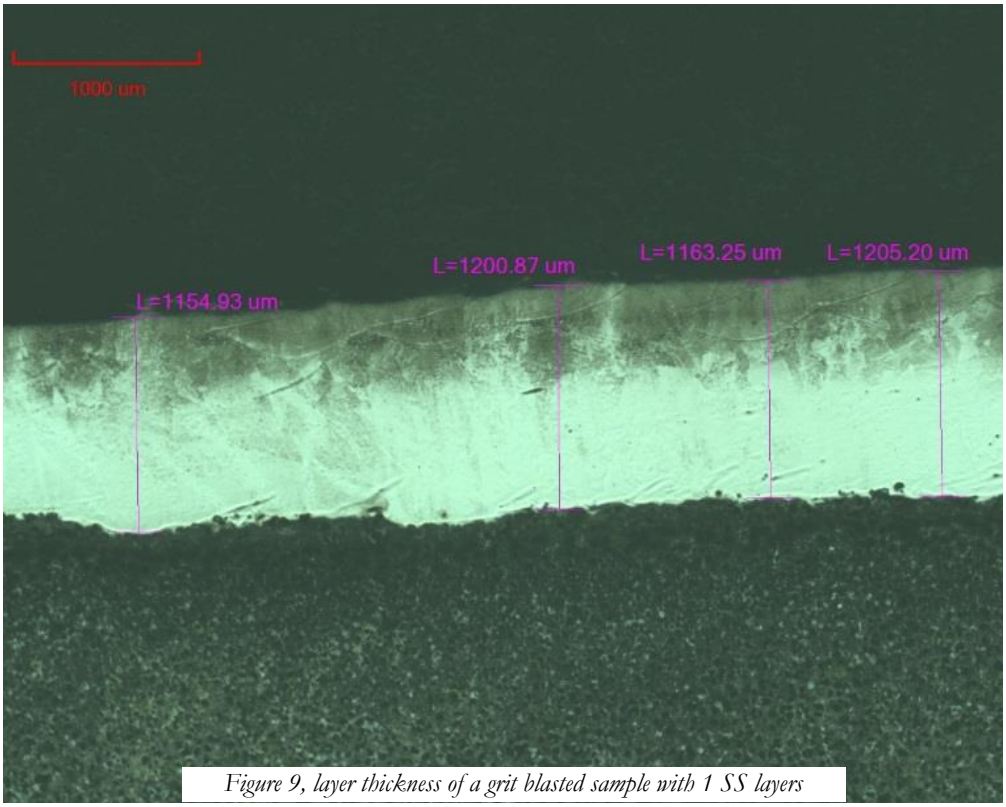

Figure 9, layer thickness of a grit blasted sample with 1 SS layers

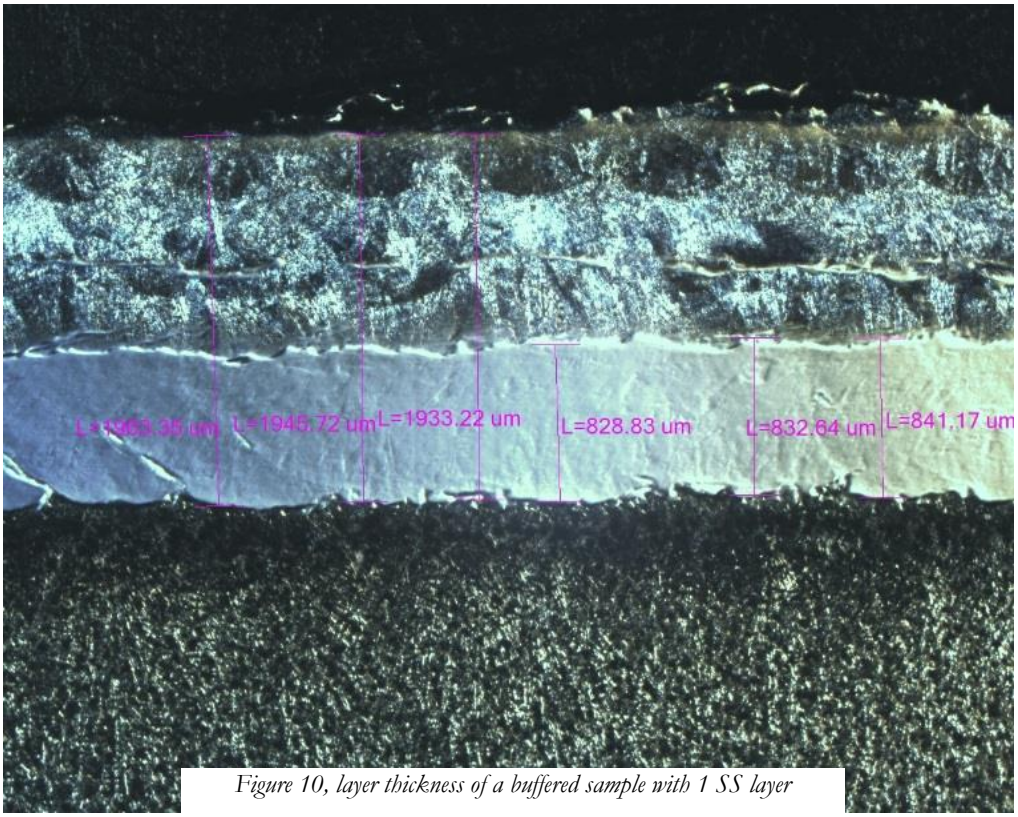

Figure 10, layer thickness of a buffered sample with 1 SS layer

Microstructure:

In a similar way to the layer thickness, the resultant microstructure does not seem to vary significantly among buffered, machined or grit blasted specimens.

In *figures 11-16* a relationship between microstructure and distance to the substrate can be appreciated. The cell size decreases as the distance to the substrate increases. There is a correlation between the gradient in cooling rates and the cell size, the faster the cooling rate the smaller the resulting cell size.

As the samples were allowed to cool down between the deposition of different layers, the mass of cold material under the last deposited layer was higher and so was the magnitude of the sink heat effect.

The resulting microstructures of *figures 17-21* show a cellular solidification pattern with small cell sizes, probably as a result of a fast cooling caused by the heat sink effect of the cast iron substrate and the previously deposited layers.

The average cell size of the surface area is significantly similar among all samples. The average cell sizes values, which were obtained using the General Interception Method, are between an ASTM Grain Size No. G 12-13. The values obtained by direct measurement of the cells with the analysing software confirm the results of the General Interception Method, as Table 4 of the ASTM E112-12 indicates that the average diameter should be between 5.6 μm (G 12) and 4 μm (G 13).

The size measurements and analysed images seem to confirm that the presence of a buffered layer or the substrate surface condition do not have a significant impact on the final microstructure of the stainless steel layers.

Even that the images may suggest that the microstructure is composed by cells of one phase embedded in a matrix of another phase because there is a strong visual contrast between the cells and the matrix, the results of the SEM/EDS analysis and ferrite measurement indicate that both cells and matrix have an austenitic structure as it was expected. The results of the ferrite measurement yielded a ferrite number between 0.5-3 for all samples.

Figures 11-13, 14-16 show how the microstructure differs depending on the distance to the substrate.

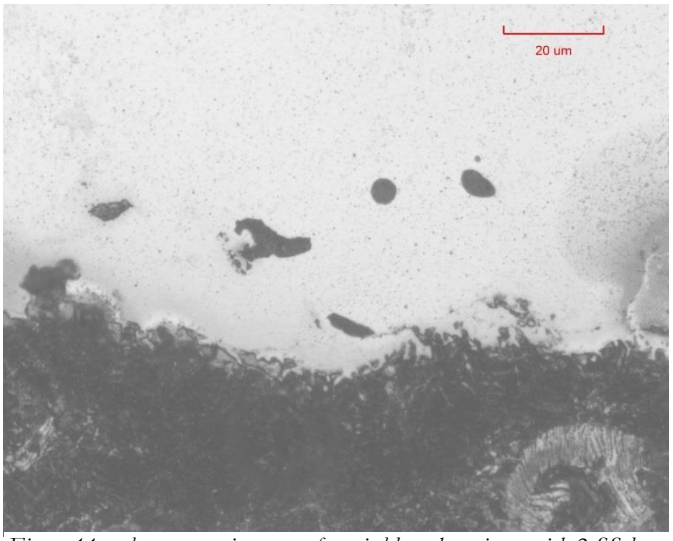

Figure 11, substrate-coating area of a grit blasted specimen with 2 SS layers

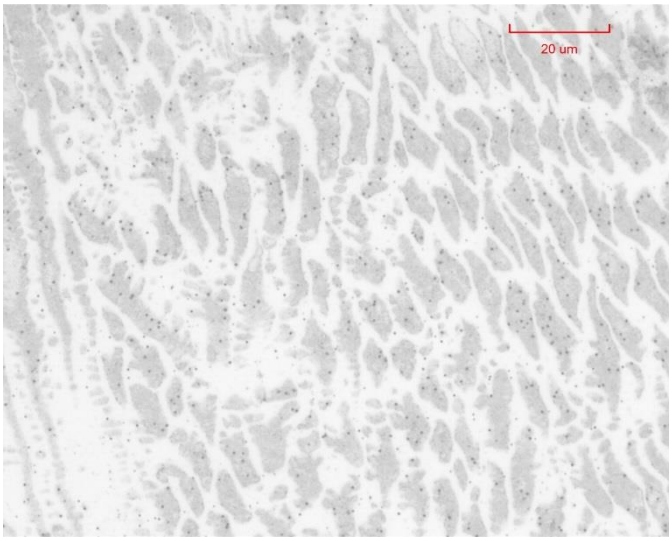

Figure 12, inter-layer area of a grit blasted specimen with 2 SS layers

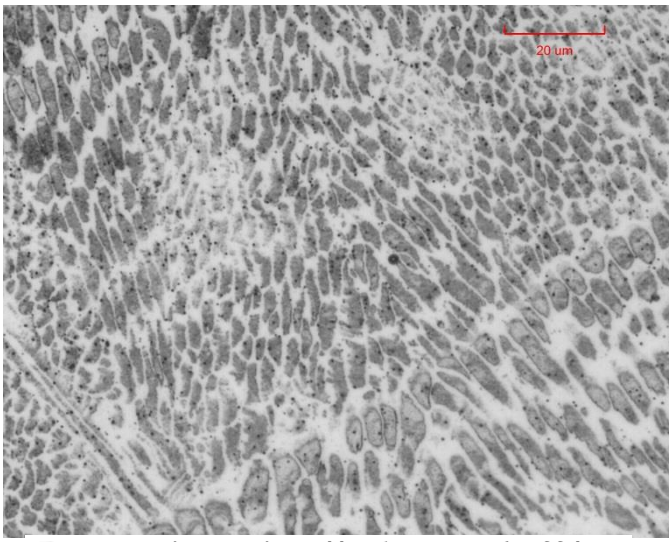

Figure 13, surface area of a grit blasted specimen with 2 SS layers

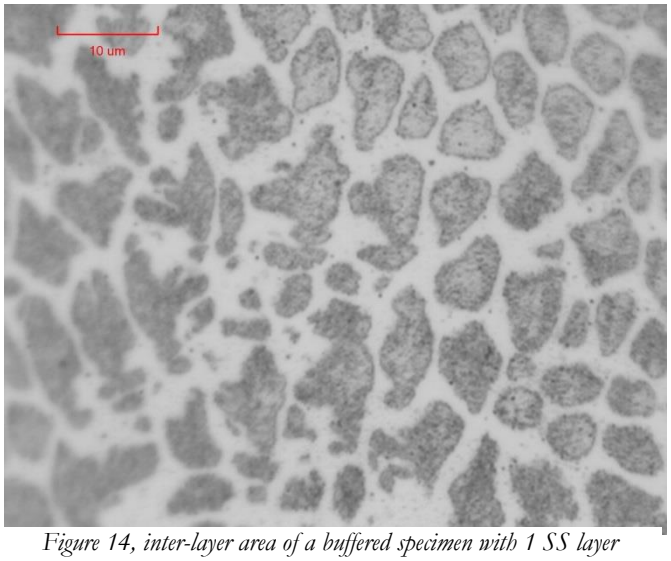

Figure 14, inter-layer area of a buffered specimen with 1 SS layer

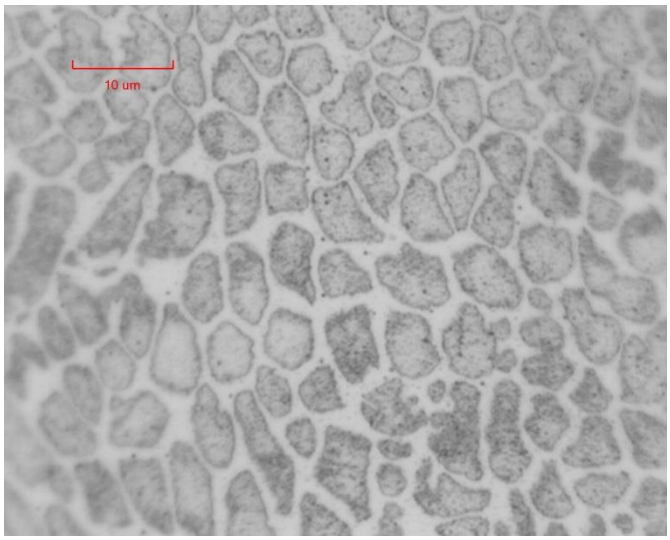

Figure 15, close to the surface area of a buffered specimen with 1 SS layer

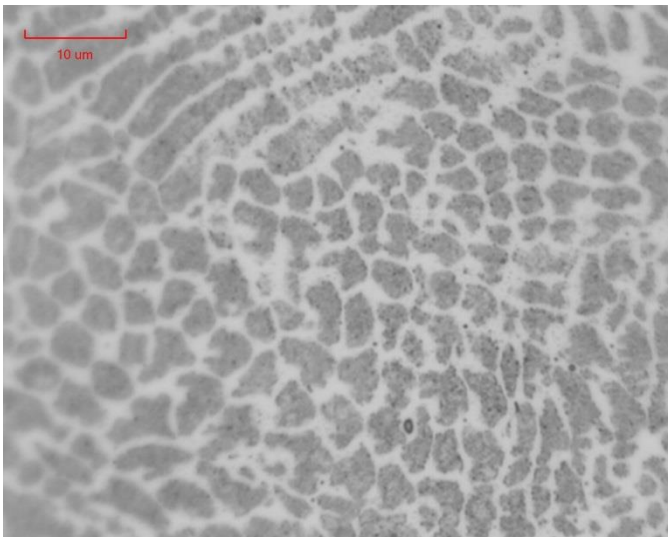

Figure 16, surface area of a buffered specimen with 1 SS layer

Figures 17-21 show the microstructure of different samples at a similar distance from the surface.

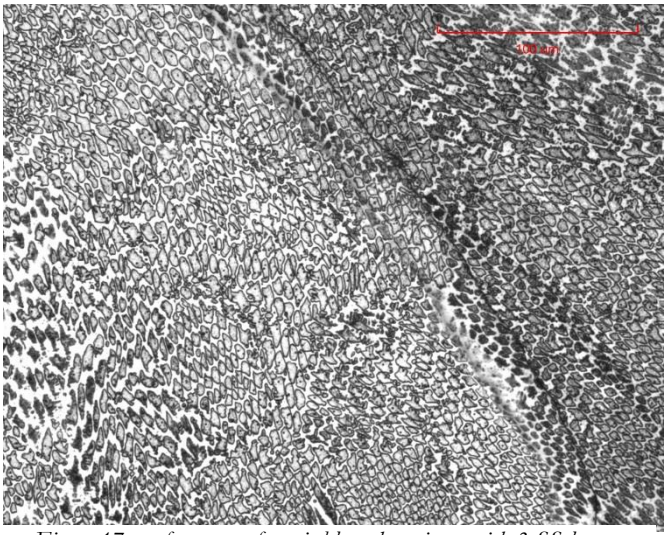

Figure 17, surface area of a grit blasted specimen with 3 SS layers

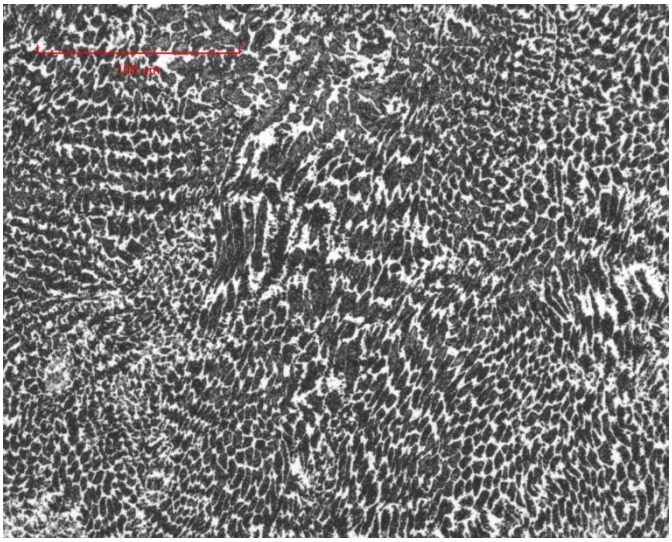

Figure 18, surface area of a buffered specimen with 2 SS layers

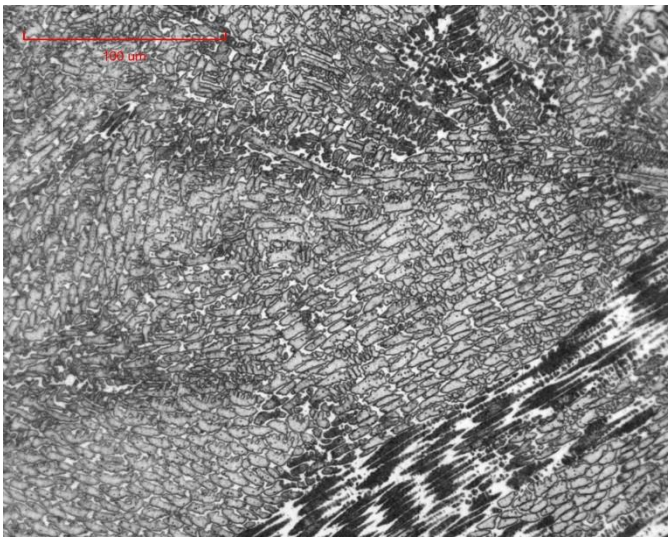

Figure 19, surface area of a machined specimen with 3 SS layers

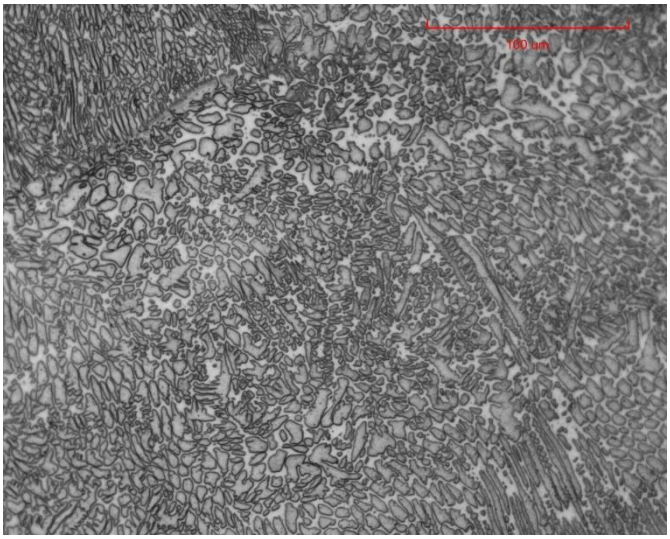

Figure 20, surface area of a buffered specimen with 1 SS layer

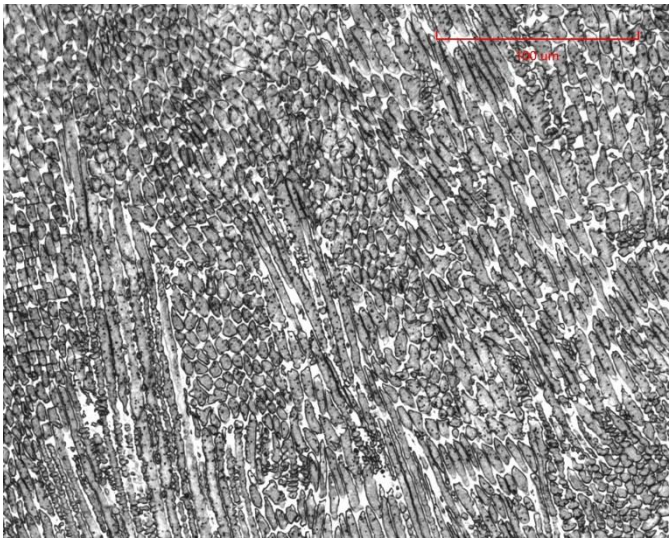

Figure 21, surface area of a machined specimen with 2 SS layers

Figures 22-23 contain direct cell size measurements at a high magnification of two specimens.

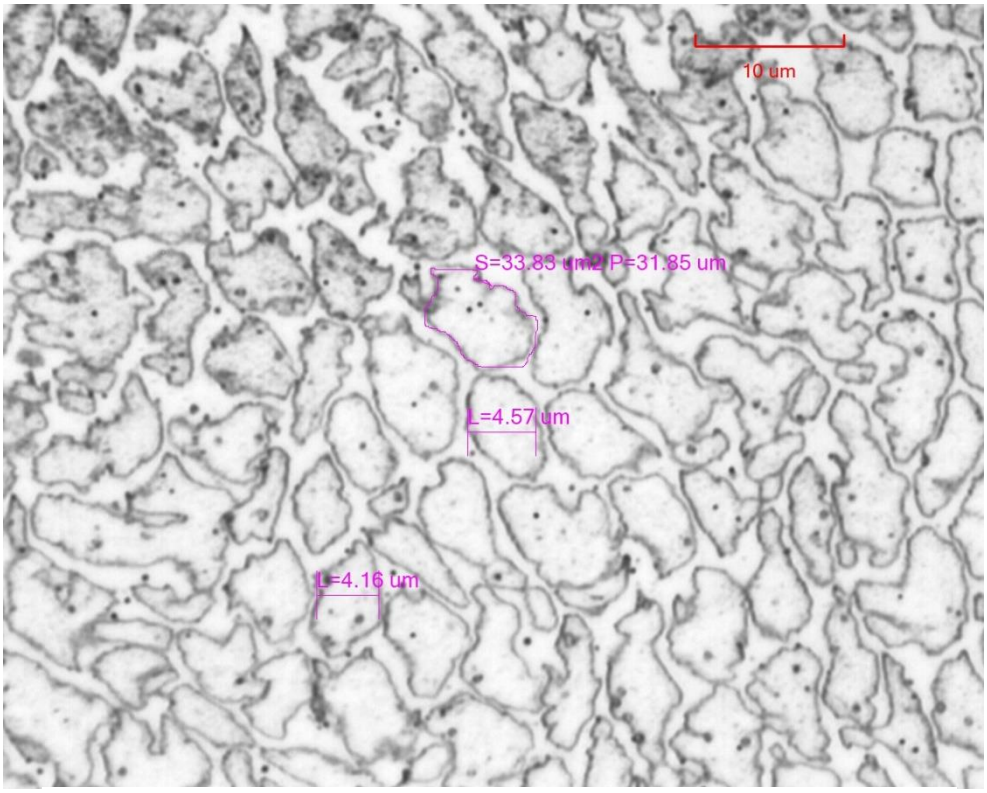

Figure 22, direct cell size measurements of the surface area of a machined specimen with 1 SS layers
Measured diameters: 4.57 μm and 4.16 μm Measured area: 33.83 μm²

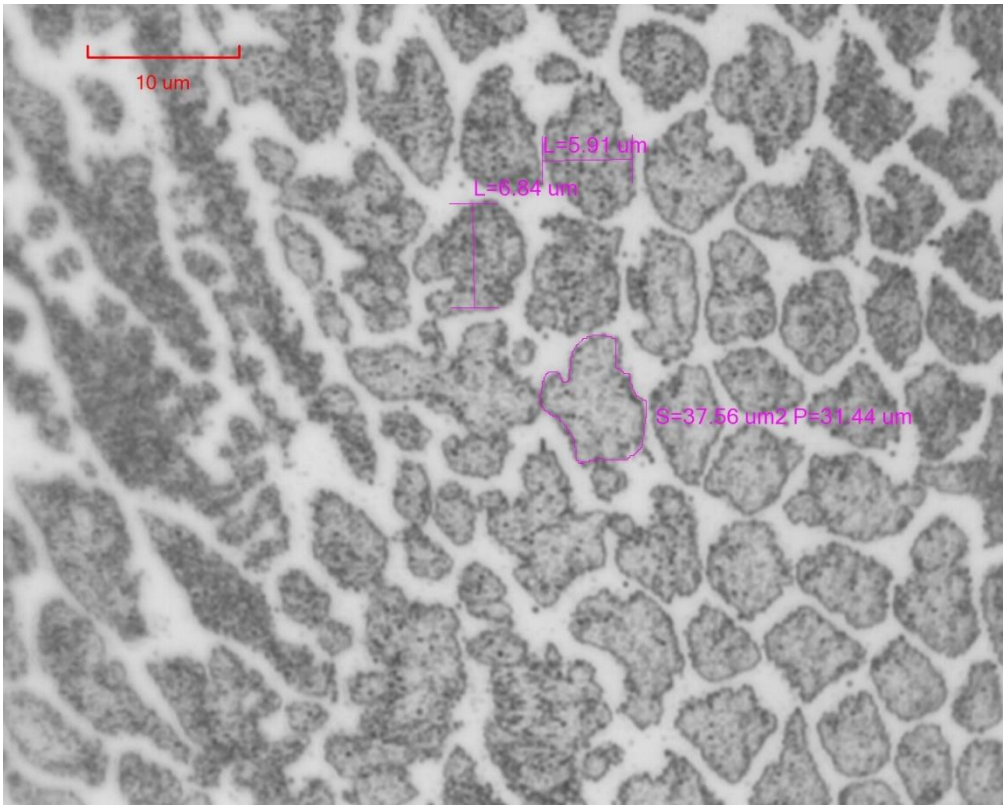

Figure 23, direct cell size measurements of the surface area of a machined specimen with 3 SS layers
Measured diameters: 6.84 μm and 5.91 μm Measured area: 37.56 μm²

Figure 24-25 are examples of the average cell size measurement following the ASTM Intercept Procedure.

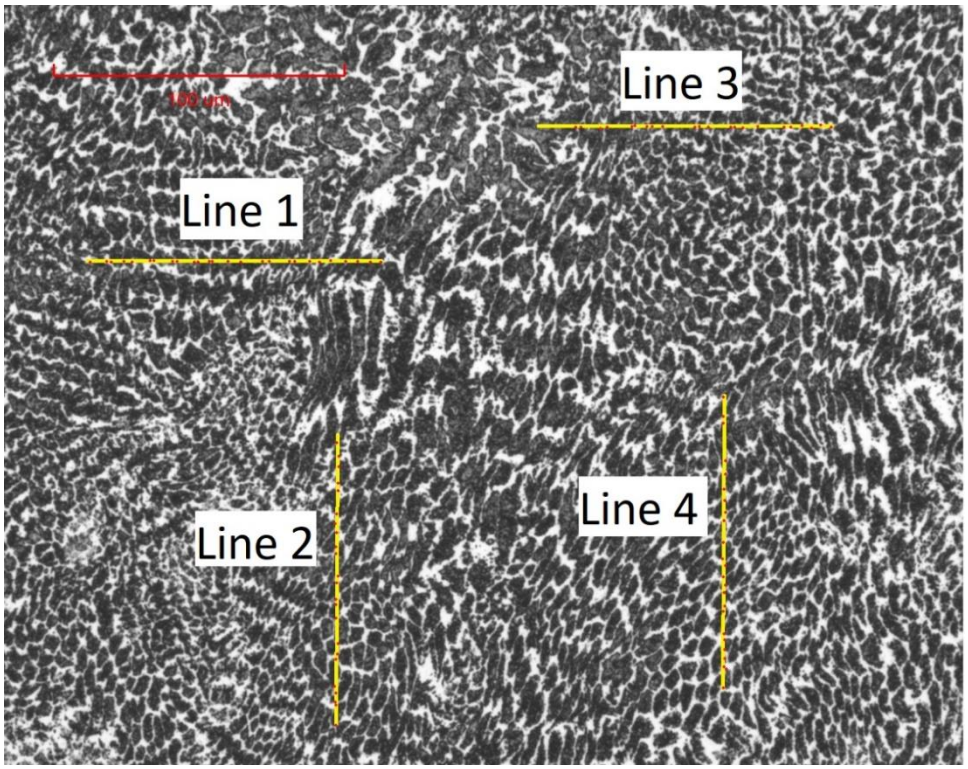

Figure 24, ASTM Intercept Method cell size measurements on the surface area of a buffered specimen with 2 SS layers

Calculated Cell Size No.: G=12.5

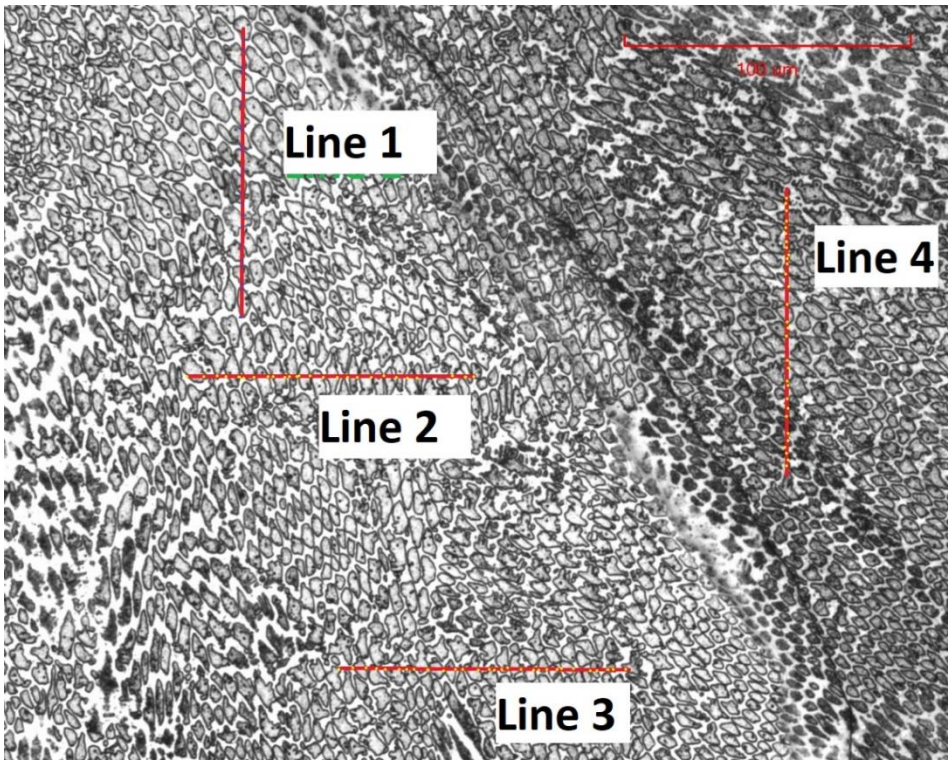

Figure 25, ASTM Intercept Method cell size measurements on the surface area of a grit blasted specimen with 3 SS layers

Calculated Cell Size No.: G=12.8

Cracking and voids:

All samples contained some microscopic voids in the substrate-layer or layer-layer interphases. The biggest observed void (*Figure 28*) had a diameter of approximately 90 μm.

Two specimens, a grit blasted specimen with 2 SS layers and a machined specimen with 2 SS layers, had horizontal cracks following the interphase between the first and the second SS layers.

Taking into account how the detected cracks seem to follow the interphase between layers, the defects may be a lack of fusion between the different layers. Another possible cause related to the previous conclusion about the austenitic structure of the specimens is solidification cracking. Solidification cracking, a type of hot cracking, is a common issue during the welding of austenitic stainless steels [27] [28].

The corrosion resistance performance of the coating was not found to be affected by the presence of voids or cracks and the bonding strength between layers was enough to resist the impact of the high pressure water jet during the wash down tests.

Figures 26 and 27 contain some examples of the detected voids and *Figures 28-31* from the horizontal cracks.

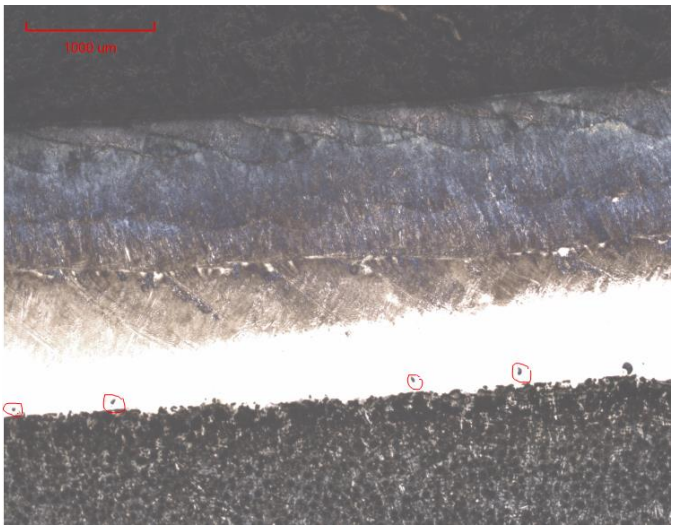

Figure 26 detected voids in a machined and remelted specimen with 2 SS

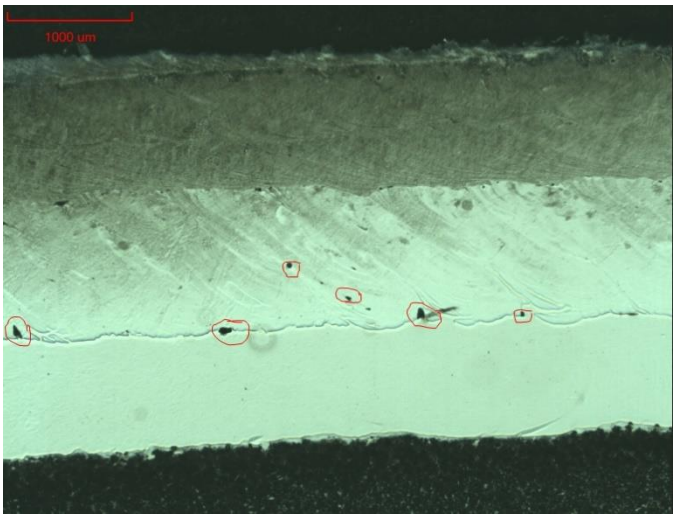

Figure 27, detected voids in a buffered specimen with 2 SS layers

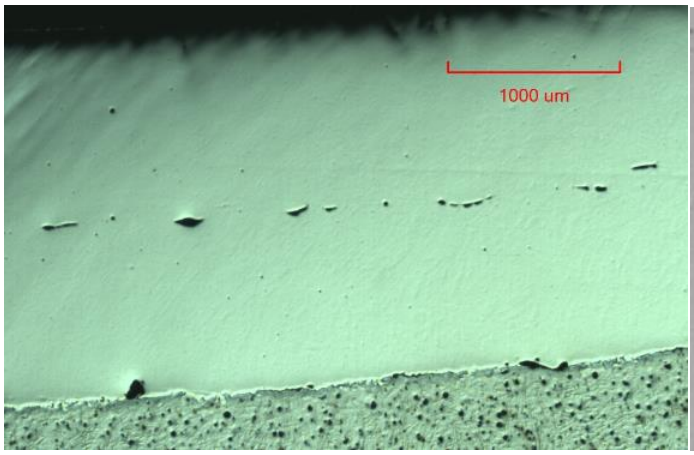

Figure 28, voids and crack in a grit blasted specimen with 2 SS layers

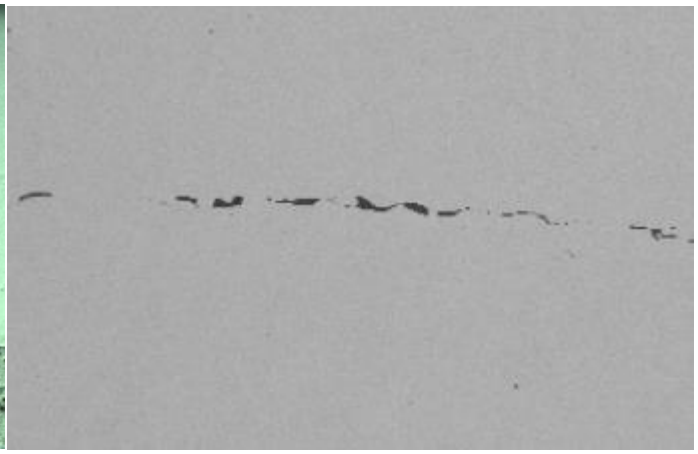

Figure 29, SEM of voids and crack in a machined specimen with 2 SS layers

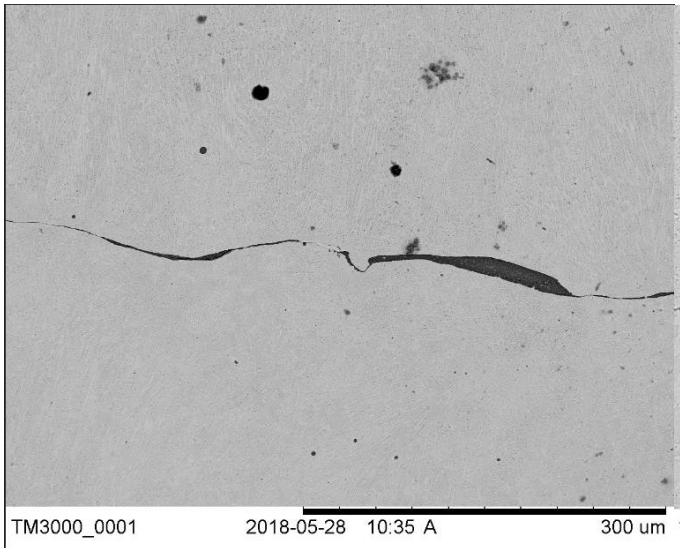

Figure 30, SEM of voids and crack in a grit blasted specimen with 2 SS layers

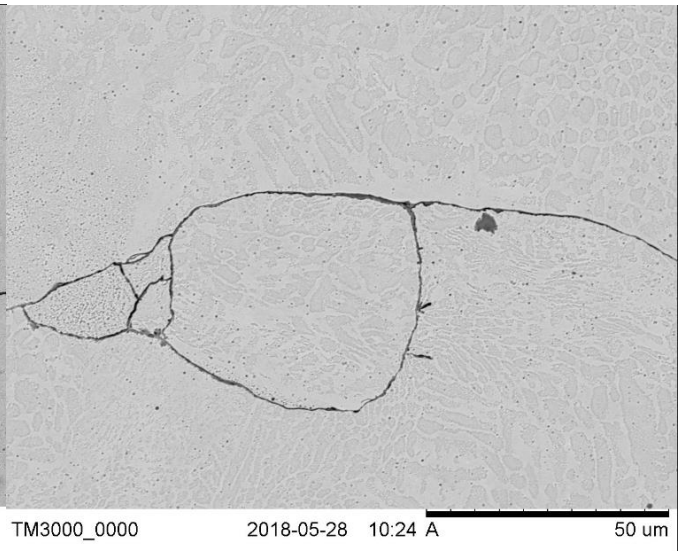

Figure 31, SEM of voids and crack in a machined specimen with 2 SS layers

4.1.2. SEM/EDS

The data provided by the EDS analysis was critical to understand the diffusion behaviour between the different materials in the sample and to conclude if LMPD is a suitable method for depositing stainless steel on cast iron.
The data provided by the system was not enough to obtain the exact chemical composition of a point, but it was able to determine the differences in chemical composition of each zone of the specimen.

Figures 32-33, 34-35, 36-37 show the results of an EDS line scan of three different specimens.

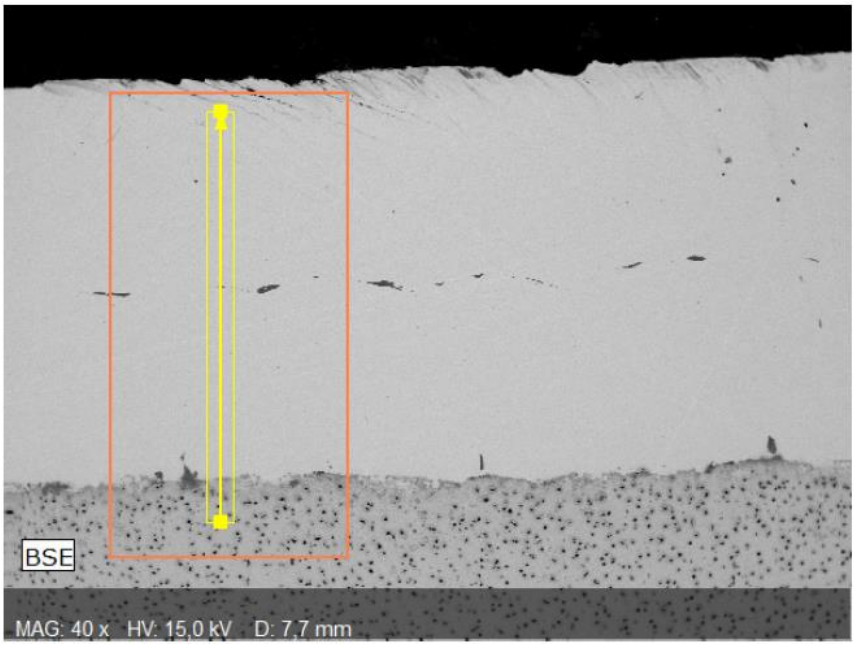

Figure 22, position of the EDS line scan on a grit blasted specimen with 2 SS layers

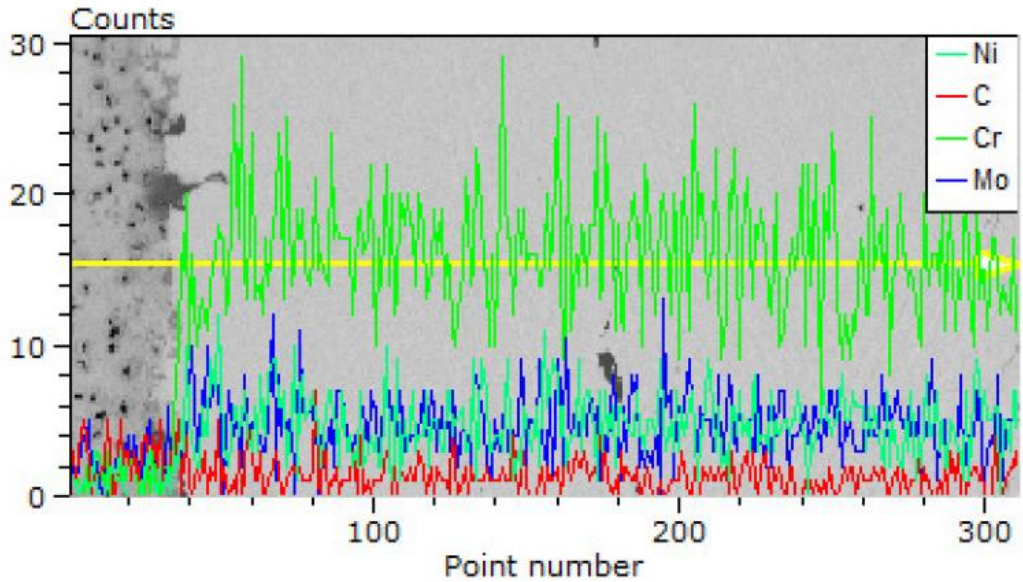

Figure 33, results of the EDS line scan on a grit blasted specimen with 2 SS layers

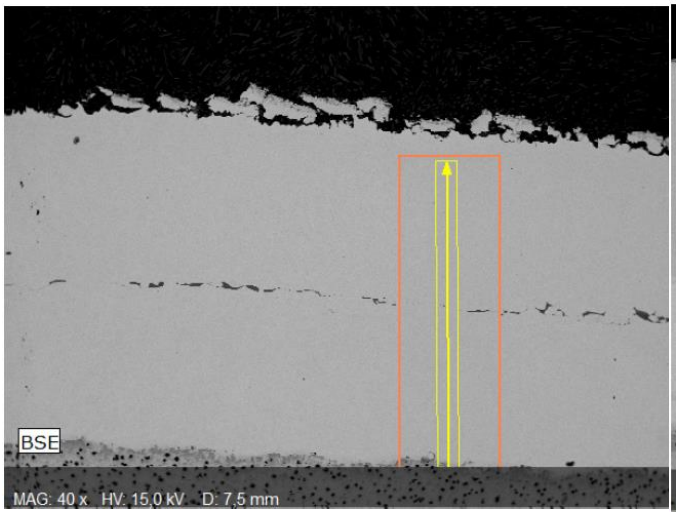

Figure 34, position of the EDS line scan on a machined specimen with 2 SS layers

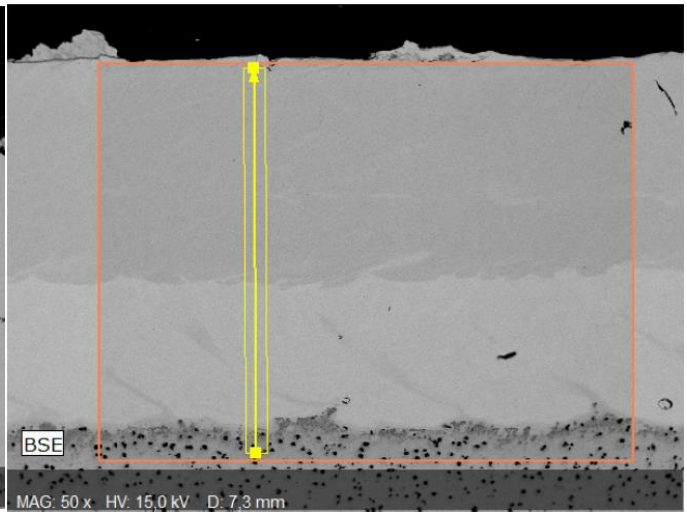

Figure 36, position of the EDS line scan on a buffered specimen with 1 SS layer

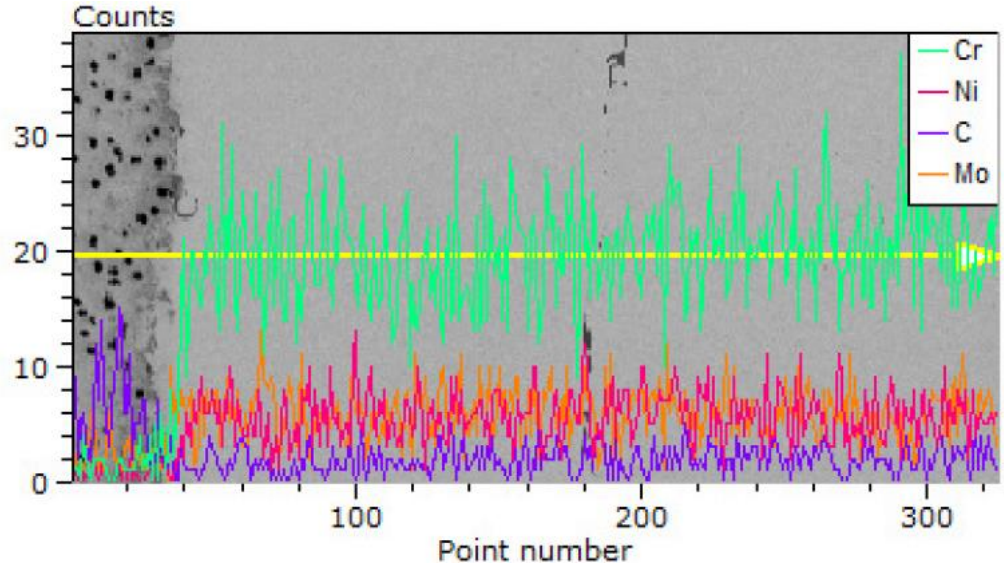

Figure 35, results of the EDS line scan on a machined specimen with 2 SS layers

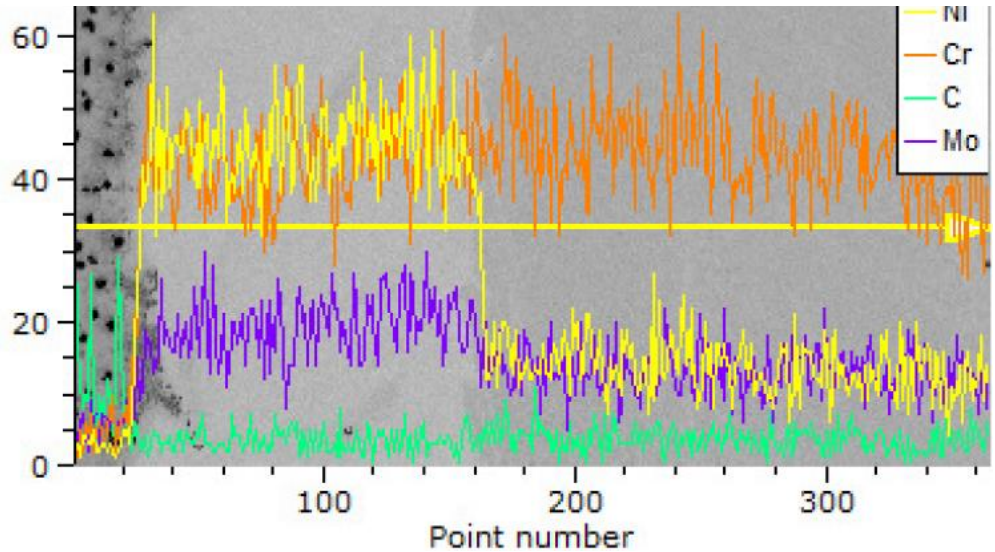

Figure 37, results of the EDS line scan on a buffered specimen with 1 SS layer

The sudden change of the chemical composition in the interphase area detected by the line scans confirm that the chemical diffusion between substrate and coating was low. This lack of diffusion can be related to the characteristic fast cooling rates and shallow penetration of LMPD processes.

The short transition from the high carbon content of the cast iron to the low one of the 316L means that the thickness of the deposited layers could be reduced without foreseeable detrimental effects on the corrosion performance of the coating. The line scan results suggest that a 316L surface with few impurities could be achieved just some millimetres away from the substrate.

If the line scan of *figure 37* is compared to the ones of *figures 35 and 33*, the use of a nickel-rick buffer layer can be considered unnecessary. The carbon content of the SS layers of the non-buttered specimens is not higher and the chemical composition of the SS surface is expected to be the same independently of the presence of a buffer layer.

4.2. Wash Down Test

All samples passed the wash down test. No effects of the wash down test were appreciated on the samples and all samples looked the same before and after the wash down test.

As the microscopic analysis of the samples did not detected any major substrate-coating weld defects in any sample, the pressures involved in the wash down test were not expected to cause any damage to the samples.

4.3. Corrosion Test

No signs of pitting corrosion were appreciated on the surface of the samples after a complete one-week long cycle.

As the microscopy and EDS analyses suggested that the chemical composition of the 316L surface had not been altered, no signs of corrosion were expected after the exposure of the samples to the corrosion cycle.

5. Conclusion

- Corrosion resistant AISI 316L SS coatings can be deposited on spheroidal graphite cast iron by LMPD. The deposited coatings successfully protected the substrate during the salt spray chamber corrosion test and the integrity of the coatings is not expected to fail during the washing procedures applied in industry.

- All coatings deposited without the use of a nickel-rich buffer layer fulfilled the acceptance criteria. Both buffered and non-buffered samples presented sound and similar microstructures.

- SEM/EDS results show that the diffusion of carbon from the carbon-rich cast iron to the SS coating was significantly low as a result of the low penetration and dilution achieved during the LMPD process.

- A completely austenitic microstructure was achieved on the surface of one-layer SS coatings due to the low diffusion. All coatings, independently of the number of layers, presented an austenitic microstructure.

- No differences were observed in terms of corrosion resistance or microstructure between samples with a machined cast iron surface and samples with a grit blasted surface. The thickness of the layer does not vary depending of the substrate.

5.1. Future Work and Research

It would be interesting to repeat the experimental methodology of this project but with a range of different process parameters. The main goal should be to reduce the thickness of the deposited layers in this project, which is probably more than enough to protect the cast iron component, while maintaining a low penetration and dilution of the SS with the substrate. The new process parameters should also reduce the amount of voids and avoid any kind of cracking in the coating.

5.2. Generalization of the result

The obtained results can be easily generalised to any industrial field apart of the F&B industry which uses austenitic stainless steel as the main contact surface material in their factories, such as the pharmaceutical and chemical industries.
The capability of combining a long-term reliable corrosion coating to a cheap and castable material such as cast iron without the use of an expensive nickel buffer layer opens all kind of possibilities to all kind of manufacturers. Probably, the limiting factors to the usage of the investigated coatings are the equipment cost, the necessity of highly educated workers and the complexity of automatizing the handling of the component for the coating of curved and complex geometries.

6. References

[1] ISO 20653:2013 Road Vehicles – Degrees of protection IP Code – Protection of electrical equipment against foreign objects, water and access

[2] Volvo Car Corporation Standard VCS 1027 1449, Accelerated Corrosion Test - Cyclic atmospheric corrosion test with salt load, 2014

[3] The Association for Packaging and Processing Technologies (2017) "2017 Trends in food processing: Market Research Report"

[4] European Hygiene Engineering and Design Group (EHEDG) Document No. 8 (2018). Hygienic Design Principles

[5] M. Pascual, C. Ferrer, E. Rayón "Weldability of spheroidal graphite ductile cast iron using Ni/NiFe electrodes", Revista de Metalurgia, Vol. 45, pp 334-338, 2009

[6] R. K.Bhatnagar, G. Gupta "A review on weldability of cast iron", International Journal of Scientific & Engineering Research, Vol. 7, Issue 5, May 2016

[7] F. Arias-González et al. "Fiber laser cladding of nickel-based alloy on cast iron", Applied Surface Science, Vol. 374, pp 197-205, 2016

[8] H. Liu et al. "Microstructural evolution and bonding characteristic in multi-layer laser-cladding of NiCoCr alloys on compacted graphite cast iron", Journals of Material Processing Technology, Vol. 232, pp 153-164, 2016

[9] Y. Li et al. "Phase evolution of ductile iron during laser cladding processing", Surface & Coatings Technology, Vol.339, pp 37-47, 2018

[10] K.Y. Benyounis et al. "Surface melting of nodular cast iron by Nd-YAG laser and TIG", Journals of Material Processing Technology, Vol. 170, pp 127-132, 2005

[11] M. Ebrahimniaa et al. "Effect of cooling rate and powder characteristics on the soundness of heat affected zone in powder welding of ductile cast iron" , Materials and Design, Vol.33, pp 551-556, 2012

[12] A. Segerstark "Laser Metal Deposition using Alloy 718 powder: Influence of Process Parameters on Materials Characteristics", PhD Thesis, University West, 2017

[13] C.-M. Lin, A. S. Chandra, L. Morales-Rivas, S.-Y. Huang, H.-C. Wu, Y.-E. Wu & H.-L. Tsai "Repair welding of ductile cast iron by laser cladding process: microstructure and mechanical properties", International Journal of Cast Metals Research, 27:6, pp 378-383, July 2014

[14] American Iron and Steel Institue (2011) A Designers' Handbook Series Nº9014: Design Guidelines for the Selection and Use of Stainless Steel, distributed by Nickel Development In-stitute.

[15] International Molybdenum Association (ed.)(2010) Practical Guidelines for the Fabri-cation of High Performance Austenitic Stainless Steels, co-published by the International Mo-lybdenum Assosiaction, the International Chromium Development Association and the Nickel Institute.

[16] J. Dutta Majumdar, A. Pinkerton, Z. Liu , I. Manna , L. Li "Mechanical and electrochemical properties of multiple-layer diode laser cladding of 316L stainless steel", Applied Surface Science, Vol. 247, pp 373–377, 2005

[17] Q. Chiao et al "On the enhanced corrosion resistance of a selective laser melted austenitic stainless steel", Scripta Materialia, Vol. 141, pp 94-98, 2017

[18] Mi. Maa, Z. Wanga, X. Zeng "A comparison on metallurgical behaviors of 316L stainless steel by selective laser melting and laser cladding deposition", Materials Science & Engineering A, Vol. 685, pp 265-273, 2017

[19] P. Guo et al "Study on microstructure, mechanical properties, and machinability of efficiently additive manufactured AISI 316L stainless steel by high-power direct laser deposition", Journals of Material Processing Technology, Vol. 240, pp 12-22, 2017

[20] P. Ganesh et al "Studies on the pitting corrosion resistance and sensitization in laser rapid manufactured specimens of type 316L stainless steel", Materials and Design, Vol. 39, pp 509-521, 2012

[21] R. K. Dayal, N. Parvathavarthini, B. Raj "Influence of metallurgical variables on sensitisation kinetics in austenitic stainless steels", International Materials Reviews, 50:3, pp 129-155, 2005

[22] T. Belleze et al. "Study of Localized Corrosion of AISI 430 and AISI 304 Batches Having Different Roughness", Metals, 8:4, pp 244, 2018

[23] S. Dadbakhsh , L. Hao, C. Y. Kong "Surface finish improvement of LMD samples using laser polishing", Virtual and Physical Prototyping, 5:4, pp. 215-221, 2010

[24] E. Yasa, J. Kruth "Application of laser re-melting on selective laser melting parts", Advances in Production Engineering & Management, Vol. 6, pp. 259-270, 2011

[25] S. Marimuthu et al "Laser polishing of selective laser components", Internation Journal of Machine Tools and Manufacturer, Vol. 95, pp. 97-104, 2015

[26] Z. When et al "Diode laser cladding of Fe-based alloy on ductile cast iron and related interfacial behavior", Surface and Coatings Technology, Vol. 286, pp. 64-71, 2016

[27] ASTM Standard E112, 2012, "Standard Test Methods for Determining Average Grain Size", ASTM International, West Conshohocken, PA

[28] V. Shankar, T. P. S. Gill, S. L. Mannan, S. Sundaresan "Solidification cracking in austenitic stainless steel welds", Sahadna, Vol. 28, pp 359–382, 2003

[29] V. Quiroz, A. Gumenyuk, M. Rethmeier, "Investigation of the hot cracking susceptibility of laser welds with the controlled tensile weldability test", Journal of Strain Analysis for Engineering Design, Vol. 47, pp 587–599, 2012